PHILOSOPHICAL TRANSACTIONS OF THE ROYAL SOCIETY A MATHEMATICAL, PHYSICAL & ENGINEERING SCIENCES

Experimental Measurements of Dimensionality and Spatial Coherence in the Dynamics of a Flexible-Beam Impact Oscillator

J. P. Cusumano, M. T. Sharkady and B. W. Kimble

Phil. Trans. R. Soc. Lond. A 1994 **347**, 421-438
doi: 10.1098/rsta.1994.0052

Experimental measurements of dimensionality and spatial coherence in the dynamics of a flexible-beam impact oscillator

By J. P. Cusumano, M. T. Sharkady and B. W. Kimble

Department of Engineering Science and Mechanics, The Pennsylvania State University, University Park, PA 16802, U.S.A.

Experiments on a flexible-beam impact oscillator are described in which the spatial structure of typical motions is explored. The beam is held in a fixed mount with clamped-free boundary conditions, and the beam is driven by impacts between its free end and a sinusoidally driven impactor. Bifurcation diagrams using impactor frequency and offset as the bifurcation parameter are obtained using a computer-driven data acquisition system. The dimensionality of the system is studied by analysis of delay-reconstructed time series of experimental data. Valid delay reconstructions are obtained using mutual information and false nearest neighbour algorithms, and the correlation dimensions is estimated for the resulting experimental attractors. The relation of these topological characterizations of the system to the spatial structure of the vibrations is studied using two-point spatial correlation measurements and the proper orthogonal decomposition. It is shown that over 90% of the mean square response amplitude is captured by the first proper orthogonal mode for the cases examined and that the spatial coherence measurements can be used to distinguish between responses with similar dimensionality.

1. Introduction

First principles formulations of solid-mechanical systems invariably result in mathematical models consisting of coupled, nonlinear partial differential (or integro-differential) equations which have infinite dimensional phase spaces. This 'curse of dimensionality' (a phrase coined by Bellman in the context of data analysis (Breiman *et al.* 1984)) causes difficulties in at least three ways important to engineers. First, even given recent advances in computational power and those which can be expected in the near future, direct simulations of such infinite dimensional systems using, for example, nonlinear finite element codes are virtually incapable of answering certain fundamental dynamical questions. In particular, parameter studies, bifurcation analyses, determination of attractor invariants and basins of attraction are simply far too time consuming for high-dimensional systems, even with the best vector/parallel codes. Secondly, even infinitely fast computation would leave a researcher or designer with a mathematical model whose complexity mirrors that of the natural world: simplified models that might explain observed phenomena may be obscured by excessive detail in the 'exact' simulation. Finally, if one is interested in designing integrated controllers for precision structural systems (such as aircraft), the complexity of the task will be directly related to the number of

Phil. Trans. R. Soc. Lond. A (1994) **347**, 421–438
Printed in Great Britain

degrees of freedom needed to capture the observed or expected dynamics of the problem.

It is therefore of central importance in nonlinear structural dynamics to determine the dimensionality of the system: what is the minimal number of degrees of freedom or 'modes' needed to describe an observed motion? And what are the characteristics of these degrees of freedom? Given the importance of the dimensionality question, it becomes equally important to identify suitable model problems that can be used for combined experiment/numerical/analytical studies. Elementary vibration theory suggests that many degrees of freedom will be excited by impacts on flexible structures. Furthermore, impact oscillators can be designed to be essentially linear between impacts, and to exhibit a wide range of dynamical behaviours with relatively small response amplitudes: these features ease, respectively, the burdens on the analyst and the experimentalist. Thus, flexible impact oscillators appear to be ideal for explorations into the relation between temporal and spatial complexity in nonlinear structural dynamics.

Impact oscillators have already proved to be theoretically important and technologically useful examples of mechanical, discrete time nonlinear dynamical systems. Many recent investigations have examined impacting systems, both from theoretical and experimental points of view (see, for example, Holmes 1992; Shaw 1985*a*, *b*; Everson 1986; Whiston 1987, 1992; Moon & Shaw 1983; Tufillaro & Albano 1986; Kowalik *et al.* 1988; Hendriks 1983; Franaszek & Isomäki 1991; Nordmark 1991; Foale & Bishop 1992). However, previous studies of the nonlinear dynamics of impact oscillators have involved systems with, either literally or effectively, one degree of freedom. This is a severe limitation since flexibility effects should be expected to play an important role in applications.

In this paper, an experimental study of a flexible-beam impact oscillator is presented. The system consists of a lightly damped thin steel beam with one end in a rigid clamp and the other end free. The free end is made to strike an impactor which vibrates sinusoidally. In most previous studies of impact oscillators, a driven or self-excited oscillator is made to strike a fixed rigid boundary, whereas in our case the impactor is driven and the beam vibrates freely between impacts. Thus the system can perhaps best be thought of as an infinite-dimensional version of the bouncing ball problem (Holmes 1992), except, of course, that elasticity replaces gravity as the source of the restoring force. An automated data acquisition system is used to obtain bifurcation diagrams for the system using impactor frequency and offset as the bifurcation parameters. The dimensionality of the system is studied using delay-reconstructed time series of experimental data. Valid delay reconstructions are obtained using mutual information and false nearest neighbour algorithms, and the correlation dimension of various attractors is estimated. The relationship of these topological characterizations of the system to the spatial structure of the vibrations is studied using two-point spatial correlation measurements and the proper orthogonal decomposition. To the best of our knowledge, this work represents the first experimental application of this technique to solid-mechanical systems (numerical application of the proper orthogonal decomposition to a 10 degree of freedom impact oscillator can be found in Cusumano & Bai 1993). The number of shape functions ('proper orthogonal modes') needed to capture most of the signal power in the response is obtained and compared to the predictions of the dimension theory. We demonstrate that the spatial coherence measurements can be used to distinguish between different motions with similar dimensionality and to identify

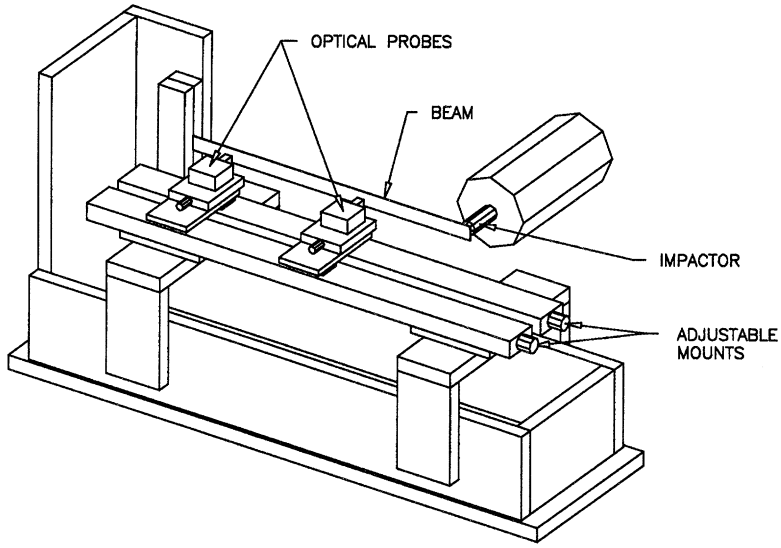

Figure 1. Schematic diagram of the experimental system. The beam tip bounces on a sinusoidally driven impactor.

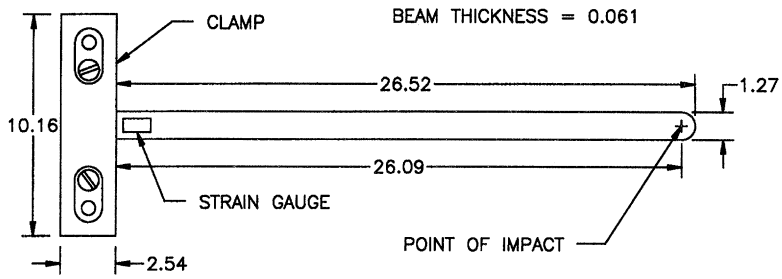

Figure 2. Beam–clamp assembly (all units are in centimetres).

dominant modes of vibration, even when linear modal analysis should be expected to fail.

In the next section of the paper the experimental system is described. In §3 experimental bifurcation results are presented: the system appears to be chaotic over most of the frequency range examined. In §4 the dimensionality of the system is explored using correlation dimension estimates. After a brief introduction to the proper orthogonal decomposition, §5 presents proper orthogonal modes obtained for several steady states. The number of significantly excited modes needed to capture the observed dynamics gives an independent measure of dimensionality. A discussion of our results and concluding remarks are presented in §6.

2. Description of the experimental system

The experimental system is a lightly damped thin steel beam (0.061 cm × 1.27 cm × 26.52 cm) with a mass of 16 g. The beam is mounted in a horizontal cantilevered position (see figures 1 and 2): the cross-sectional axis corresponding to the smallest bending stiffness is oriented vertically so that the motion is confined to the horizontal plane. The beam is made to vibrate by striking its free end with a sinusoidally

Table 1. *Natural frequencies and modal critical damping ratios for the experimental system*
(The modal damping equals $4\pi f_n \zeta_n$.)

mode n	natural frequency f_n/Hz	modal critical damping ratio, ζ_n
1	7.31	1.4×10^{-2}
2	44.5	4.5×10^{-4}
3	125	4.2×10^{-4}
4	246	3.8×10^{-4}
5	407	3.4×10^{-4}
6	608	4.9×10^{-4}
7	849	1.9×10^{-4}

vibrating impactor which consists of a 2.2 kg mass driven by an electromagnetic shaker. The impactor has an axisymmetric, approximately spherical tip. Unless otherwise noted, the impactor was positioned so that it just touched the end of the undeformed beam when the system was at rest. Two reflectance-compensated optical fibre displacement probes are used to obtain data from the beam. The sensors are mounted on precision adjustable sliders that allow each of the probes to be positioned independently along the length of the beam to an accuracy of 0.025 mm. The main advantage of the moving impactor configuration used here (as opposed to one in which the beam is driven and the impactor is replaced by a rigid stop) is that absolute displacement measurements can be made while the optical probes remain stationary: this avoids excessive vibration of the sensors and optical fibre leads, and hence minimizes measurement noise and instrumental drift. A third optical probe is used to acquire displacement data from the impactor.

Baseline characterization of the system was provided by the natural frequencies and modal damping ratios of the non-impacting beam (see table 1), which were obtained by attaching the beam–clamp assembly (so that the error associated with remounting the beam would not be a factor) to an electromagnetic shaker. The shaker was excited with low-level random noise and the response of the beam was measured via a pair of strain gauges mounted near the clamped end of the beam. The signal from an accelerometer mounted on the shaker and the strain signal were routed to a PC-based signal analyser which computed the required transfer function. All data acquisition and signal generation for these and other measurements was performed with 12-bit A/D and D/A converters.

Bifurcation diagrams were obtained with an automated data acquisition, workstation-based system. The data acquisition control program was written with Fortran 77 and a real-time data acquisition subroutine library. A digitally generated sine wave, output from the computer, drove the shaker amplifier to generate the bifurcation diagrams. A chosen bifurcation parameter (such as driving frequency) was incremented until the parameter range of interest was swept through. At each step, after waiting a fixed number of periods for transients to die off, the signal from an optical probe positioned at the free end of the beam was sampled stroboscopically, again for a fixed number of periods, in phase with the driving sine wave. More precisely, bifurcation data was collected in a Poincaré section determined by the positive slope zero crossing of the driving signal. Because the Poincaré section is defined mathematically by the phase of the impactor motion, not the phase of the

PHILOSOPHICAL TRANSACTIONS OF THE ROYAL SOCIETY A MATHEMATICAL, PHYSICAL & ENGINEERING SCIENCES

driving signal, the frequency response characteristics of the shaker cause the actual phase of the Poincaré section to change (in a continuous, predictable manner) as the frequency is scanned. Similarly, the frequency response of the shaker causes the impactor amplitude to vary across the range of the bifurcation diagram. Details of these shaker frequency response effects are discussed in the next section. The same bifurcation procedure was carried out on the impactor itself to verify that mechanical feedback was minimal (i.e. that the response of the impactor was merely periodic throughout the frequency range of the bifurcation diagrams).

The power spectral density was obtained from optical probe signals for various trial runs at several frequencies. These showed that, to the resolution of our data acquisition, 100% of the signal power was contained in a bandwidth of less than 1000 Hz. Accordingly, all signals for time-domain data were low-pass filtered at 1000 Hz (by elliptical filters with 115 dB/octave rolloff) to eliminate out of band noise. The frequency domain measurements used anti-aliasing filters integral to the signal processing unit. Ambient observational noise for this setup was measured with the shaker excitation signals turned off and found to be about 1 least significant bit (2.44 mV root mean square for the A/D scaling used).

To build the spatial correlation matrix needed for the proper orthogonal decomposition (the covariance R_{ij}, discussed in greater detail in §5), a series of two-point spatial correlation measurements need to be made using the two optical probes. Five equally spaced points were chosen along the beam (giving a 5×5 covariance matrix) and two-point spatial correlation measurements were made for all possible combinations of these points by

$$R_{ij} = \langle (x_i - \bar{x}_i)\,(x_j - \bar{x}_j) \rangle, \tag{1}$$

where x_i is the displacement at the ith point along the beam and i and j range from 1 to 5. The angle brackets denote the time average and the overbar indicates the mean value. The sliders were used to move manually the two optical probes to different points along the length of the beam: the time-consuming nature of this part of the process is essentially what limited the data collection to five measurement points for this work. Each run took about 2 h, and increasing the number of nodes to ten would increase the total data collection time to 8 h. A control program running on the data acquisition workstation calculated the covariance of the signals from the two optical probes over a 30 s time interval. The program was run ten times for each combination of probe positions and the average was used as the entry in the correlation matrix. The standard deviation from the mean of the ten values was used to form an error matrix E_{ij}, which provides a measure of the error in each entry of R_{ij}.

3. Bifurcation diagrams

A dynamic bifurcation diagram was made by holding the input voltage to the shaker amplifier constant at 2.0 V and varying the frequency from 5 Hz to 100 Hz in 395 steps. At each frequency step, 200 periods of transient data were skipped before 100 points of stroboscopically sampled displacement data were collected. The resulting bifurcation diagram is shown in figure 3*a*. A bifurcation diagram with increased resolution, generated by sweeping from 5 Hz to 50 Hz in 716 steps, is shown in figure 3*b*. The step sizes were approximately uniform. However, they varied slightly over the frequency range due to peculiarities in the clocks used to control the data acquisition.

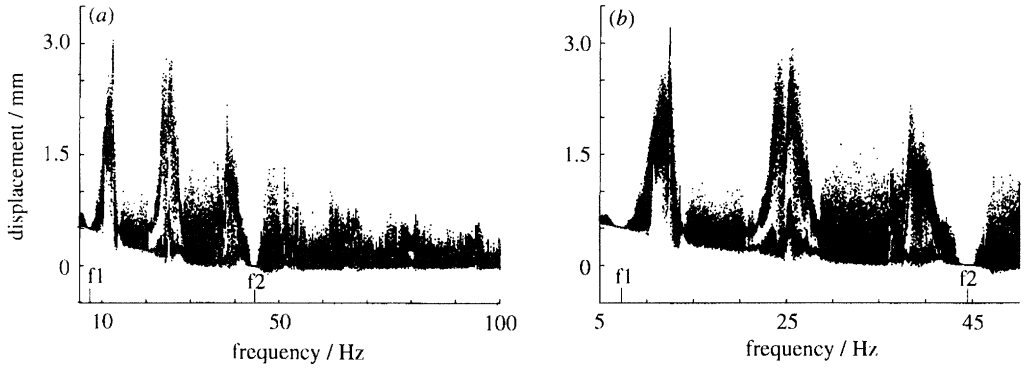

Figure 3. Frequency bifurcation diagrams for the system with constant shaker input of 2 V and zero offset: (*a*) 5 Hz to 100 Hz in 395 steps; (*b*) 5 Hz to 50 Hz in 716 steps. The first two natural frequencies, f_1 and f_2, are marked for reference.

Two features of the diagrams should be kept in mind by the reader. First, the shaker linear frequency response results in a phase shift of about 138° at 5 Hz with respect to the driving signal, tapering off to 19° at 50 Hz and −2.5° at 100 Hz. The Poincaré section used to collect data at each fixed frequency in figure 3 must therefore be interpreted accordingly, since data was collected at zero phase of the driving signal. Secondly, the diagrams represent system behaviour along a curved path in the impactor amplitude/frequency parameter space. While the input to the shaker was kept at a constant voltage amplitude, the impactor displacement amplitude changed throughout the frequency range due to the shaker frequency response. At 5 Hz the impactor amplitude is 0.585 mm and drops to 6.18×10^{-2} mm at 50 Hz and 1.26×10^{-2} mm at 100 Hz. (At frequencies above 100 Hz the shaker is nominally a 'constant force' device and hence, the impactor displacement amplitude varies approximately as f^{-2}, where f is the forcing frequency. All of our experimental work had excitations at less than 100 Hz, however.) Despite these complications the bifurcation diagrams correctly present the qualitative features of the motions, as well as quantitative features such as relative response amplitudes.

The bifurcation structure indicates that the system behaviour is complex (apparently chaotic) over most of the frequency range studied, with the exceptions being two small periodic régimes which coincide with the first two natural frequencies of the non-impacting beam ($f_1 = 7.31$ Hz, $f_2 = 44.5$ Hz). At these frequencies, the impactor and the beam tip remain in contact at all times so no impacting occurs. Power spectra of the beam tip displacement signal at the first two natural frequencies verify that these orbits are indeed periodic. It is interesting that, despite what one might expect from linear vibration theory, excitation of the impact oscillator near the natural frequencies results in regular motions of relatively small amplitude, when compared with motions at other driving frequencies. We speculate that periodic motions occur at the natural frequencies because a single mode dominates in the steady-state response. Since the natural frequencies for bending vibrations are not integer multiples of one another, only single mode free vibrations are periodic, and hence, it is easier for the single mode vibrations to synchronize with the impactor motion to give a periodic response in the impacting system (see §6 for further discussion).

Another interesting feature of the bifurcation diagrams is the régime of large amplitude chaotically modulated period-2 orbits that appear near $f = 25$ Hz

PHILOSOPHICAL TRANSACTIONS OF THE ROYAL SOCIETY A MATHEMATICAL, PHYSICAL & ENGINEERING SCIENCES

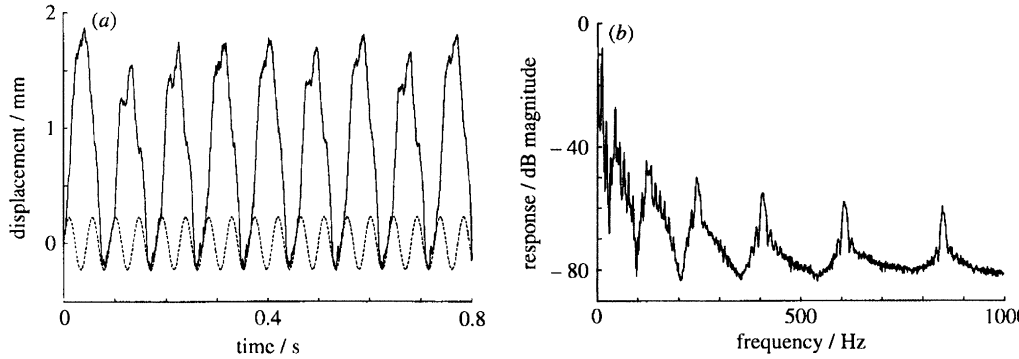

Figure 4. Chaotically modulated period-2 response at $f = 22$ Hz: (*a*) time series of beam tip (the sinusoidal impactor motion is shown by the dashed line); (*b*) power spectrum of tip response.

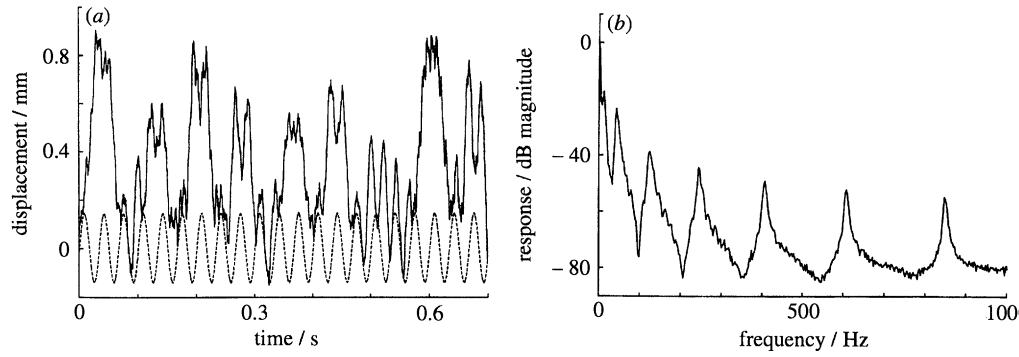

Figure 5. Chaotic response at $f = 30$ Hz: (*a*) time series of beam tip (the sinusoidal impactor motion is shown by the dashed line); (*b*) power spectrum of tip response.

(throughout this paper, the periodicity of various orbits is given with respect to the impactor period). Response data taken at an impactor frequency of $f = 22$ Hz are shown in figure 4. Figure 4*a* clearly shows the basic period-2 character of the motions: the large amplitude tip motion, though modulated, contacts the impactor every two forcing periods. The broad band spectrum in figure 4*b* is consistent with what one expects for a chaotic response. Figure 5 shows similar results for an impactor frequency of $f = 30$ Hz. No regularity is apparent in this case but the power spectrum is surprisingly similar to the period-2 chaotic motion. In particular, notice that in both cases peaks occur in the power spectra at the natural frequencies of the non-impacting system. (This is especially clear above 200 Hz.) This type of response was found to be typical of the motions for the system.

The effect of shaker zero position (or 'offset') was examined with bifurcation diagrams taken at $f = 22$ Hz and using the same 2 V shaker input used for figure 3. With a constant impactor amplitude of 0.300 mm, the offset was varied from -0.9 mm to 0.9 mm in 709 steps. The first 900 impactor periods were discarded as transients before collecting the next 100 periods of data for the diagram. In figure 6*a* the diagram obtained by increasing the offset is shown. For offsets substantially less than minus the impactor amplitude (-0.300 mm), the steady-state motion of the beam is merely the trivial solution in which the impactor and beam do not touch. At an offset equal (within experimental precision) to minus the impactor amplitude, a grazing bifurcation (Nordmark 1991; Foale & Bishop 1992) occurs

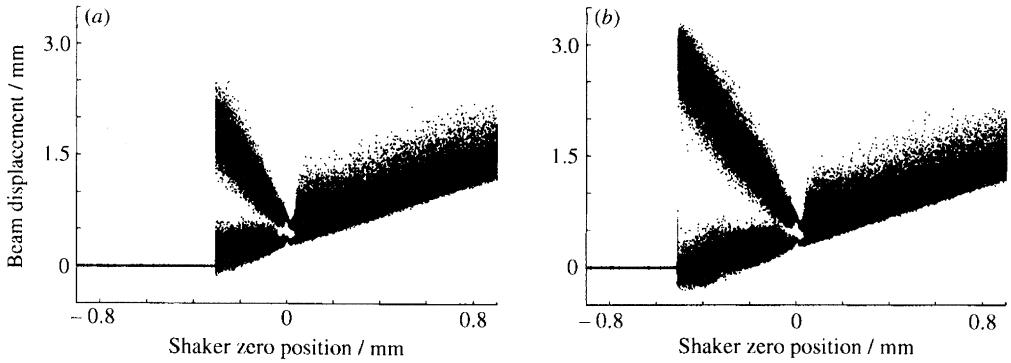

Figure 6. Offset bifurcation diagrams for the system with shaker input of 2 V and $f = 22$ Hz: (a) increasing offset (marked as 'zero position' in figure); (b) decreasing offset.

straight into a chaotically modulated period-2 motion. (The actual onset of the impacting motion was measured at -0.305 mm. The 0.005 mm difference is near the limit of our ability to identically calibrate the impactor and beam optical probes but we also suspect that aerodynamic effects may trigger the impacting slightly before the actual grazing bifurcation.) A branch of these motions continues as the offset is increased, giving rise to the motion at $f = 22$ Hz shown in figure 4 when the offset reaches zero. The period-2 chaotic branch ends and a branch of chaotic motions with no obvious periodicity becomes attracting at an offset of about 0.04 mm. In figure 6b the diagram is generated with decreasing offset. The diagram is identical to figure 6a, except that the chaotically modulated period-2 branch is seen to persist when the offset is decreased below the original grazing bifurcation point. This hysteretic behaviour indicates that the system has at least two basins of attraction for offsets between approximately -0.5 mm and -0.3 mm. Though many attempts were made to manually perturb the system onto other solutions, this was the only instance of multi-basin behaviour found during these experiments.

The remainder of this paper deals with the results that were obtained with the offset set equal to zero.

4. Dimension estimates

The development of fractal dimension theory and, in particular, of the correlation dimension algorithm (Grassberger & Procaccia 1983), has allowed dimensionality to be studied in physical and numerical experiments on a variety of fluid-mechanical and solid-mechanical systems. (Numerous examples can be found in the book by Moon (1992) and in the references therein.) From our point of view, the utility of fractal dimension estimates lies in the following: given a motion on an attractor with fractal dimension d, the number of phase space dimensions m needed to contain the attractor is bounded by

$$[d] \leqslant m \leqslant 2[d]+1, \tag{2}$$

where $[a]$ denotes the next greatest integer to a. The upper bound is due to Mañé's theorem (Mañé 1981) which states that 'typical' coordinatizations of a phase space containing an attractor of dimension d will leave the attractor lying in a subspace of dimension no greater than $2[d]+1$. Mañé's theorem specifically uses the capacity dimension, d_0, as its dimension measure: we compute the correlation dimension, d_C, which is a lower bound to d_0, and use it to put bounds on the dimensionality of the system via inequality (2).

Dimension estimates were carried out for three impactor frequencies corresponding to the periodic orbit ($f = 7.2$ Hz), the chaotically modulated period-2 orbit ($f = 22$ Hz) of figure 4 and the chaotic orbit ($f = 30$ Hz) of figure 5. At each frequency, 150000 points of beam tip displacement data were collected at a sampling rate of 5000 Hz. The time series were delay-reconstructed (Packard *et al.* 1980; Takens 1981) in the usual manner: let the sampled time series of N points be given by

$$\{x_1, x_2, x_3, \ldots, x_N\}. \tag{3}$$

Then a sequence of m-dimensional delay-reconstructed state vectors,

$$\boldsymbol{y}^j = (y_1^j, y_2^j, \ldots, y_m^j), \tag{4}$$

can be formed for a fixed delay δ by letting

$$y_i^j = x_{j+\delta(i-1)} \tag{5}$$

for $1 \leqslant i \leqslant m$ and $1 \leqslant j \leqslant N_y$, where $N_y \equiv [N - \delta(m-1)]$. The embedding dimension m must be chosen large enough so that the mapping defined by the delay embedding procedure is invertible: for a known phase space dimension n, Taken's theorem states that generic values of δ are guaranteed to give good results as long as $m \geqslant 2n+1$. However, one typically does not know the true phase space dimension in experiments, and finite precision and noise make careful selection of δ mandatory.

For this work, the delay was chosen using the mutual information criterion of Fraser & Swinney (1986) and Fraser (1989). While we will not give the mathematical definition of the mutual information of a time series here, we remark that it can be thought of as a 'nonlinear autocorrelation': by taking the first minimum of the mutual information, the delayed coordinates are optimal in a specific information-theoretic sense. A mutual information code was run on each data set to determine the time delay δ to use for the embedding.

After computing δ, the embedding dimension m was chosen using the method of false nearest neighbours (Kennel *et al.* 1992). The basic idea in the false nearest neighbour method is to check how the distances between points in suitably defined neighbourhoods change as the embedding dimension is increased. Points which appear to be close to each other in dimension m but which become far apart in dimension $m+1$ are defined to be false nearest neighbours. Of course, in the algorithm, terms like 'nearby' and 'far apart' must be precisely defined. For this study, the embedding dimension was chosen as the dimension which resulted in less than 0.1% of the points being false nearest neighbours: points were considered to be false nearest neighbours when the euclidean distance between them increased by greater than a factor of 15 as m increased by 1. Using the value of m resulting from the false nearest neighbours algorithm (call it m_{F}), together with the previously determined value of δ, the data set was then delay-reconstructed, and the correlation dimension d_{C} was calculated. Note that the values of d_{C} and m can be checked for internal consistency from inequality (2). As a final check, d_{C} was computed for a few values of $m > m_{\mathrm{F}}$ and in all cases was found to be in good agreement with the value obtained with $m = m_{\mathrm{F}}$, as it should be.

For the periodic orbit at $f = 7.2$ Hz, which serves as our reference case, a dimension estimate of $d_{\mathrm{C}} = 1.010 \pm 0.009$ was obtained from a fit over a 20:1 scaling range. (For this and other dimension estimates, the error given is the measurement error, i.e. it is an estimate of the repeatability of the result.) The estimate was obtained using a computed delay of $\delta = 0.03$ s (150 sample steps) and an embedding

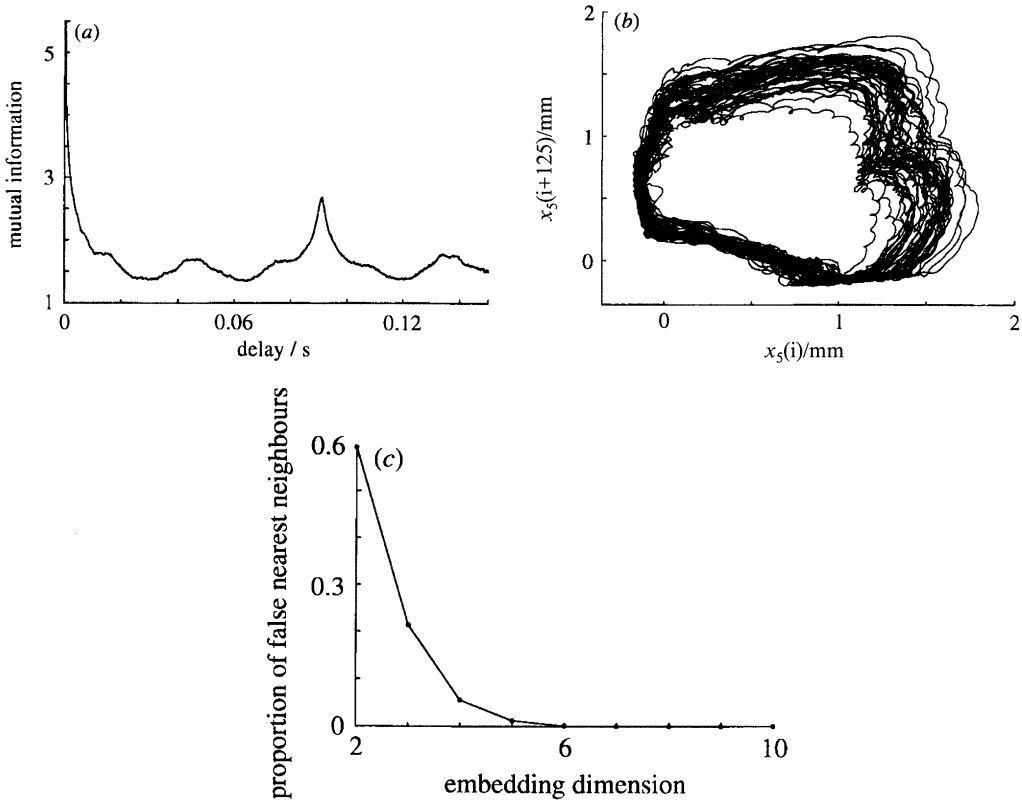

Figure 7. Delay reconstruction results for response at $f = 22$ Hz: (*a*) mutual information against delay for tip displacement data (x_5); (*b*) two dimension delay reconstruction using delay chosen from first minimum of (*a*); (*c*) proportion of false nearest neighbours against embedding dimension.

dimension of $m = 3$. This result is, as it should be, consistent with the time domain, frequency domain and delay reconstructions, all of which show a periodic orbit. (In the interest of brevity, this data is not shown.) We remark that the simple, periodic structure of the orbit is also reflected in the mutual information, which shows successive peaks of approximately constant height separated by a time delay equal to the period of oscillation. Several other embedding dimensions up to $m = 8$ were investigated, with the result being nearly the same for each.

More interesting results were obtained for the chaotically modulated period-2 orbit at $f = 22$ Hz (see figure 7). An embedding dimension of $m = 7$ with a time delay of $\delta = 0.025$ s (125 steps) was computed for this data. The log–log plot of the correlation integral $C(r)$ against the length scale r is shown in figure $9a$: d_C is defined as the 'limiting' slope of this curve for sufficiently small r. In practice, a minimum length scale is fixed by the scale of the observational noise. The curve of figure $9a$ possesses two distinct scaling regions. The upper scaling region gives a 'dimension estimate' (i.e. slope) of 1.22 ± 0.01, while the lower scaling region yields the actual estimate of $d_C = 4.0 \pm 0.1$ over a 3.7 : 1 scaling region. While the upper scaling region is not used for determining d_C (since it is not 'in the limit of small r'), it does give us information about the structure of the attractor: over a range of relatively large length scales, the attractor looks like a noisy periodic orbit, clearly visible in figure $7b$. This periodicity is also reflected by the mutual information calculation, which shows a

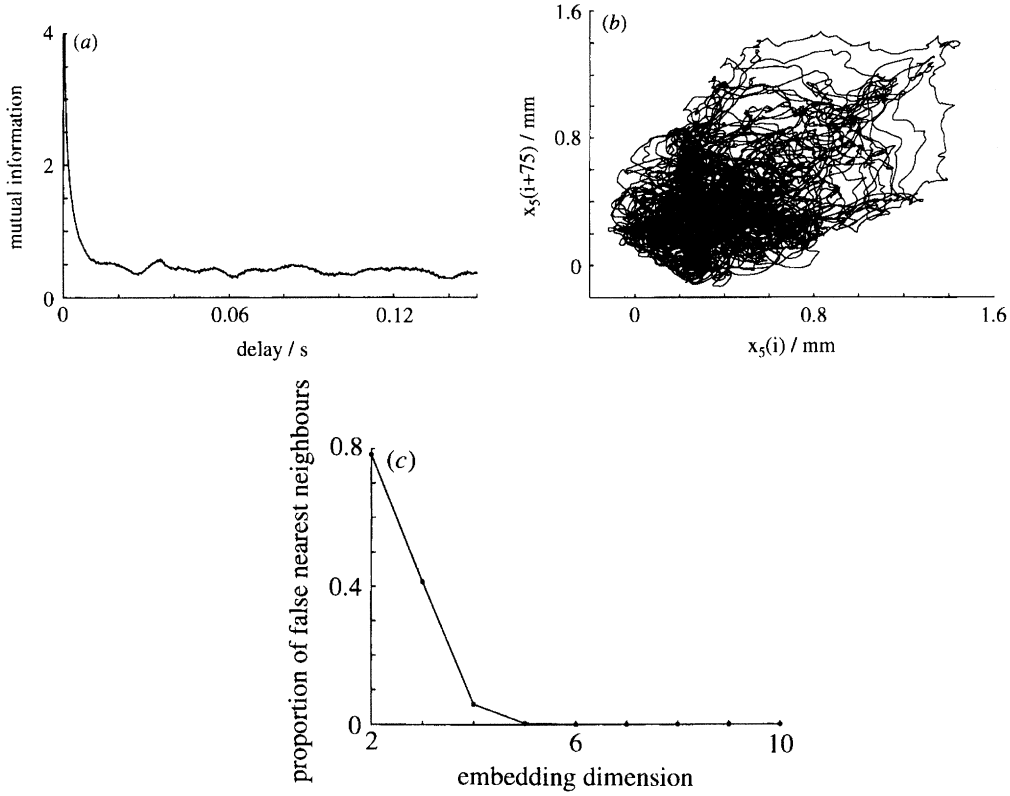

Figure 8. Delay reconstruction results for response at $f = 30$ Hz: (*a*) mutual information against delay for tip displacement data (x_5); (*b*) two dimension delay reconstruction using delay chosen from first minimum of (*a*); (*c*) proportion of false nearest neighbours against embedding dimension.

peak for a delay equal to approximately 0.091 s. This suggests a characteristic frequency of approximately $1/0.091 \approx 11$ Hz for the system, a result entirely compatible with the noisy period-2 character of the motion indicated by the bifurcation diagram.

The correlation integral curve for the orbit at $f = 30$ Hz shows only one scaling region (see figures 8 and 9*b*). The dimension estimate of $d_C = 3.83 \pm 0.08$ (over a 4.5:1 scaling region) was obtained using the computed values of $m = 6$ and $\delta = 0.015$ s (75 steps). The existence of only a single scaling region is consistent with the reconstructed orbit of figure 8*b*: unlike the orbit of figure 7*b*, no periodic structure is visible in the orbit. In this sense, one can think of the attractor as more self-similar than the attractor for $f = 22$ Hz, and thus, even though the limiting dimensionality of both attractors is close to the same value, the shape of the correlation integral curves helps us identify the two orbits as belonging to distinct states based on their large-scale structure. The lack of internal temporal structure is reflected in the mutual information plot of figure 8*a*, which shows no major peaks for non-zero delays.

We close this section by pointing out that the dimension estimates and embedding dimensions are all internally consistent, as is readily verified by substitution into inequality (2).

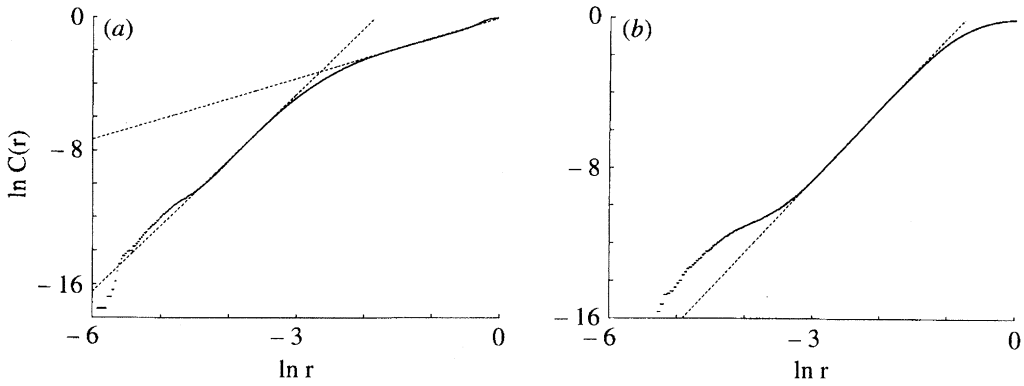

Figure 9. Correlation integral curves for the chaotic responses: (*a*) result for data of figures 4 and 7 (the correlation dimension is taken to be the slope of the lower (small r) scaling region); (*b*) result for the data of figures 5 and 8. Dashed lines indicate the fit to the scaling regions.

5. Spatial coherence measurements

While dimension theory is useful, it is only of limited value for system modellers: fractal dimension estimates give bounds on the number of degrees of freedom, but they do not indicate appropriate configuration variables to use in formulating models of the system. In particular, fractal dimensions do not yield any spatial information concerning important shape functions or modes in the system, information which is usually of great significance in engineering applications. One method for studying dimensionality that addresses some of these limitations is based on the proper orthogonal decomposition of the covariance of a random function (Loève 1963), applied originally in mechanics to the study of turbulent fluid flows (see Lumley 1967; Sirovich 1987). The object of study in the proper orthogonal decomposition (POD) method is the spatial correlation given by the dyadic product

$$\boldsymbol{R}(\boldsymbol{s},\boldsymbol{s}') = \langle \boldsymbol{x}(\boldsymbol{s},t)\,\boldsymbol{x}(\boldsymbol{s}',t)\rangle, \tag{3}$$

where $\boldsymbol{x}$ is an appropriate field variable in space $\boldsymbol{s}$ and time t.

For our purposes, the spatial correlation is the tensor given by

$$\begin{aligned}\boldsymbol{R} = \ &\langle \boldsymbol{x}(t)\,\boldsymbol{x}(t)\rangle = \langle x_i(t)\,x_j(t)\,\hat{\boldsymbol{e}}_i\,\hat{\boldsymbol{e}}_j\rangle \\ &= \langle x_i(t)\,x_j(t)\rangle\,\hat{\boldsymbol{e}}_i\,\hat{\boldsymbol{e}}_j \equiv R_{ij}\,\hat{\boldsymbol{e}}_i\,\hat{\boldsymbol{e}}_j,\end{aligned} \tag{4}$$

where $x_i(t)$ is the displacement at the ith point along the beam. Clearly, $\boldsymbol{R}$ is a hermitian tensor and thus its eigenvectors form a complete orthogonal set. Denoting the eigenvectors of $\boldsymbol{R}$ (called proper orthogonal modes, or POMS) by $\hat{\boldsymbol{\phi}}_i$ and expanding the configuration vector $\boldsymbol{x}(t)$ as $\boldsymbol{x}(t) = \Sigma\,\alpha_i(t)\,\hat{\boldsymbol{\phi}}_i$, one has $\boldsymbol{R} = \langle \alpha_i(t)\,\alpha_j(t)\rangle\,\hat{\boldsymbol{\phi}}_i\,\hat{\boldsymbol{\phi}}_j$. Since the $\hat{\boldsymbol{\phi}}_i$ are eigenvectors of $\boldsymbol{R}$, this implies that

$$\hat{\boldsymbol{\phi}}_i \cdot \boldsymbol{R}\hat{\phi}_j = \langle \alpha_i(t)\,\alpha_j(t)\rangle = \hat{\boldsymbol{\phi}}_i \cdot \lambda_i\,\hat{\boldsymbol{\phi}}_j = \lambda_i\,\delta_{ij}. \tag{5}$$

Equation (5) demonstrates that the modal amplitudes $\alpha_i(t)$ are linearly uncorrelated and the associated eigenvalues are simply the mean-square proper orthogonal modal amplitudes. (It also shows that $\boldsymbol{R}$ is positive definite.) In fact, it can be shown that the eigenvectors of $\boldsymbol{R}$ (i.e. the POMS) give mode shapes that are optimal in a least squares sense: they capture more power per mode than any other set of basis functions, a result also known as the Karhunen–Loève decomposition (Ghanem &

Table 2. *Eigenvalues of the experimental correlation matrix* R_{ij}

For each frequency, each eigenvalue is shown along with the percentage of the total power determined using its absolute value (see text for error discussion).

Eigenvalues of R_{ij}	$f = 7.2$	$f = 22$	$f = 30$
λ_1	381.49 (99.01%)	1133.69 (97.76%)	220.01 (90.98%)
λ_2	−2.96 (0.77%)	12.41 (1.07%)	19.59 (8.10%)
λ_3	0.84 (0.22%)	−11.95 (1.03%)	1.79 (0.74%)
λ_4	−0.03 (0.01%)	1.44 (0.12%)	0.36 (0.15%)
λ_5	0.00 (0.00%)	0.13 (0.01%)	0.08 (0.03%)
Largest eigenvalue of error matrix E_{ij}	2.10	16.85	7.69

Spanos 1991). The sum of the λ_i is equal to the total mean square amplitude (the 'power') of the response at the measured points and approaches the true mean square amplitude as the number of measured points increases. Thus, the POD method furnishes an alternative measure of dimensionality: the number of degrees of freedom needed to capture the observed dynamics can be estimated as the number of POMs needed to exceed a fixed fraction (say 99%) of the total power.

As discussed in §2, practical considerations limit our current implementation of this method to a relatively small number of sensor locations along the length of the beam: five sensor positions (x_1 through x_5) were located at distances of 1.96, 7.99, 14.02, 20.05, and 26.09 cm from the clamped end of the beam. Data was collected following the procedure outlined in §2: correlations were computed for each combination of sensor positions by using ten sets of 1.5×10^5 data points. Since R_{ij} is positive definite, all of the λ_i should be positive, and thus one could use the singular value decomposition to compute the λ_i and the POMs. However, we employed standard routines for computing eigenvalues and eigenvectors, since the occurrence of negative eigenvalues for R_{ij} is a useful indication of measurement error. Table 2 presents the eigenvalues of R_{ij} and the percent of the total power contained in the POD mode associated with each eigenvalue. For each of the three frequencies, the largest eigenvalue of the error matrix E_{ij} is also shown. As the table shows, only one POD mode appears above the level indicated by the largest eigenvalue of E_{ij} for an impactor frequency of $f = 7.2$ Hz. Indeed, λ_2 is spurious, as indicated by its negative sign (keep in mind, however, that positiveness does not in itself imply validity). The one valid POM (see figure 10*a*) captures over 99% of the power in the displacement signal, and thus, from the point of view of displacements, the response appears to be well modelled by a single degree of freedom. Although this is not surprising, given the simple periodic nature of the motion, we point out that this estimate is consistent with the dimensionality result in §4: the dimension of the phase space for a single-mode model is 3 (2 phase-space dimensions per mode plus time) which agrees with dimension theory via inequality (2).

The proper orthogonal decomposition applied to the data for an impactor frequency of $f = 22$ Hz again yields one POM clearly above the measurement noise. However, though λ_2 is near the noise limit of the measurement (as determined by E_{ij}), it is at least not negative. Furthermore, the second POM in this case contains a greater portion of the total power, and this seems to be reflected in the more plausible second mode shape seen in figure 10*b*. We suspect that the second POM is just visible in the noise but the dynamic range of the current experimental system appears to

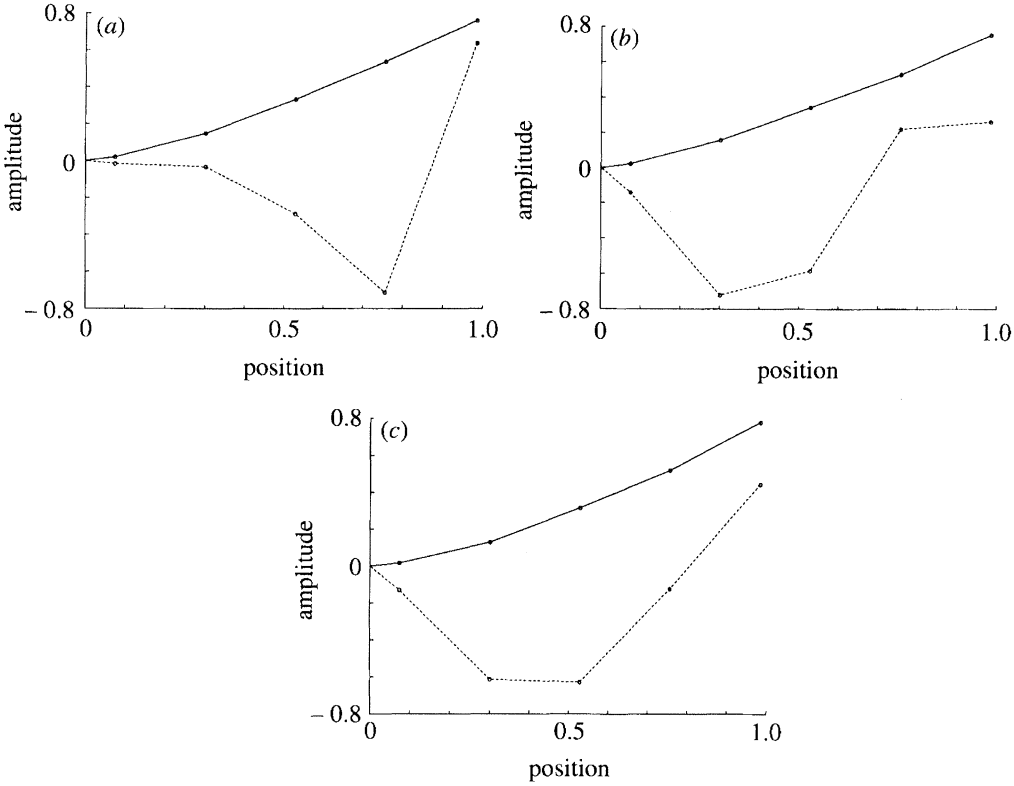

Figure 10. The first two experimental proper orthogonal modes: (*a*) periodic orbit at $f = 7.2$ Hz; (*b*) chaotically modulated period-2 orbit at $f = 22$ Hz; (*c*) chaotic orbit at $f = 30$ Hz. The first and second modes are shown by the solid and dashed lines, respectively. Circles indicate sensor locations along the beam length, which is normalized to 1. Modes are shown going to zero at the clamped end.

have difficulty picking up simultaneously the large first POM and the second POM which is about 20 dB down. The fact that 98% of the signal power is contained in the first POM, with the rest being in higher modes, gives some insight into the dual scaling regions found in the correlation integral plot for the data. Using figure 9*a* and inequality (2), the estimated dimension of the phase space is between 2 and 5 for the upper scaling region (which has a 'false' dimension of about 1.22), or between 4 and 9 for the lower scaling region (which has a 'true' dimension of about 4.0). If only the large amplitude first POM is used, a phase space dimension of 3 is obtained. This falls within the range predicted by dimension theory using only the upper scaling region for the dimension estimate and corresponds to the coarse, periodic part of the orbit. Given the true estimate of $d_C \approx 4.0$, two to five POMs are expected to be needed based on dimension theory.

The chaotic motion observed at $f = 30.0$ Hz yields two POMs above the noise floor (figure 10*c*), giving a phase space dimension of at least 5. This falls within the 4 to 9 range predicted by dimension theory, based on the estimate of $d_C \approx 3.8$. Table 2 shows that the amount of power in the first POM drops to 91% in this case and the amplitude of the second POM is only about 11 dB down from the first, but the third POM is about 21 dB down and is clearly in the measurement noise limit. Comparing figures 10*a–c*, one can see the effect of noise on the estimation of the POMs. The first modes

have amplitudes well above the noise and are essentially identical. The second POM has a kinked shape in figure 10*a*, when its amplitude is buried in the measurement error: such physically implausible shapes are found to be typical of POMS corresponding to spurious λ_i. However, the mode shape becomes smoother as its amplitude increases in figure 10*b* and 10*c*. It is reasonable to expect that the spatial structure of motions (i.e. the POMS) for the system will not be very sensitive to the particular motion used to perform the calculations, but rather, will be a system property in much the same way that linear normal modes are. (Such an assumption has been born out in numerical experiments by Cusumano & Bai (1993).) While the experimental evidence is by no means definitive, the sameness of the first POM in figures 10*a–c* supports this hypothesis. Thus, one suspects that figures 10*a–c* show the second POM emerging from the measurement noise as λ_2 increases.

6. Discussion and conclusions

In this paper we have presented an experimental study of dimensionality in an elastic impact oscillator and we have applied the proper orthogonal decomposition to study the relation between dimensionality and spatial structure for the system. While impact oscillators are technologically relevant objects of study in their own right (as, for example, common sources of noise in machinery), our main interest here has been in using them as an experimentally tractable model problem for studying spatio-temporal interaction in structural systems. The bifurcation diagrams suggest that the typical responses of such systems can be expected to be chaotic: we speculate that the common occurrence of chaotic behaviour in the system originates physically from the fact that the beam is very lightly damped and the natural frequencies for the free bending vibrations are not integer multiples of one another. Hence the many-mode free vibrations which are typical between impacts are quasi-periodic with many frequencies and it is difficult for synchronization to occur with the impactor motion. In our experiments responses with $> 99\%$ of the power in a single mode occur only near the natural frequencies, exactly where the response was periodic. (One must also keep in mind that these periodic responses were *non-impacting*, as well.) The theoretical issue, then, will be to determine precisely the conditions under which such synchronization can happen: we suspect that more complicated single and multi-mode *impacting* periodic motions do indeed exist, but have very small basins of attraction in the parameter régime studied here. (By comparison, periodic responses were found by Cusumano & Bai (1993) to be quite common in their numerical study of a lower dimensional system with damping of roughly an order of magnitude greater.)

Despite the fact that the response power spectra typically have bandwidths spanning tens of linear modes, in all of the cases studied here over 90% of the mean square response amplitude was shown to be captured by the first proper orthogonal mode. It is important to keep in mind, however, that these results are related to displacement data: strain data may yield different insights into the dynamics, since strains are directly related to the elastic potential energy of the system. From a signal processing perspective, strain gauges should be expected to amplify higher modes, since the output of gauges set up for bending measurements is, for small amplitudes, proportional to the second spatial derivative of the displacement.

From a general methodological perspective, the importance of comparing several different methods of experimental data analysis on complex signals has been

PHILOSOPHICAL TRANSACTIONS OF THE ROYAL SOCIETY A MATHEMATICAL, PHYSICAL & ENGINEERING SCIENCES

demonstrated. By combining topological methods, like dimension estimates and false nearest neighbour analysis, with the temporal analysis of the mutual information calculation and the spatial analysis provided by the proper orthogonal decomposition, subtle distinctions can be made between different stationary states, even those with similar dimensionality. Statements concerning the 'strength' of chaos in a given system must be made carefully: different measures can give quite different answers to such questions. For example, the period-2 chaos of figures 4 and 7 is 'more strongly chaotic' than the chaos of figures 5 and 7 in the sense that it has a higher correlation dimension, but it is 'less chaotic' in that it has greater temporal and spatial coherence (as indicated, respectively, by figure 6*a* and the results in table 2). Furthermore, we have shown the importance of using all of the information in the correlation integral curve: typically, the existence of multiple scaling regions is viewed as a nuisance, but from our perspective it provides significant information concerning the dimensionality of the system at different levels of coarse graining.

We have demonstrated the utility of the proper orthogonal decomposition method for structural vibration problems. For the motions encountered in this study, maximum displacements were less than a few percent of the beam length. Together with the fact that the motions were dominated by the first POM, this indicates that strains in the beam were very small and that the beam dynamics is linear between impacts. Current modelling efforts are taking this observation as a working hypothesis (the algorithm described in Cusumano & Bai 1993, can easily be applied to a suitable linear model such as that provided by the Bernoulli–Euler beam equation). However, linear frequency response measurements on the impacting system fail completely: the coherence between impactor input and beam output is close to zero. This is so because the impacting system is strongly nonlinear (there is no 'linear limit'). It is thus at first surprising that the typical chaotic power spectra (e.g. figures 4 and 5) are very close to the linear transfer function for the non-impacting beam, and, to the extent we were able to measure, the POMS are similar to the corresponding linear normal modes. We hypothesize that this 'modal correspondence' between the linear and nonlinear systems is due to a statistical similarity between the nonlinear chaotic responses and an ensemble of impulse–response tests on the non-impacting system, an idea which makes physical sense given the nature of excitation in the system. We speculate that the deliberate excitation of chaotic impacting responses may thus be of practical use for engineering modal analysis. This is especially true since the proper orthogonal decomposition is more general than standard modal analysis methods since it makes no reference to linearity: being entirely based on statistics, it will yield useful information even when the response between impacts is nonlinear.

The number of POMS above the measurement noise was found to give an independent dimensionality estimate (using two phase space dimensions per mode plus one dimension for time) that was consistent with the predictions of dimension theory. However, the small number of sensor locations that it was practical for us to use and the limited dynamic range of the POM estimate with the current experimental setup prevent us from making more definite statements on the modal dimensionality of the system. The vexing problem of limited dynamic range in the proper orthogonal mode calculation is the main area targeted for improvement in current efforts. The signal to noise ratio at beam tip sensor was about 60 dB so the reason for the relatively poor performance of the POM estimates (20 dB dynamic range) is not clear: we suspect that the long time (about 2 h) required to move the two sensors manually

PHILOSOPHICAL TRANSACTIONS OF THE ROYAL SOCIETY A MATHEMATICAL, PHYSICAL & ENGINEERING SCIENCES

to the different locations is introducing non-stationarity into the data and that wave-born mechanical coupling between the sensors and the bouncing beam is a greater noise source than first anticipated. We hope to build future versions of this experiment using many sensors (about 10–20) with better mechanical isolation, which will be able to collect all of the needed data in a few minutes. A more fundamental issue is related to the impulsive nature of impact oscillations, which tends to make the system dimensionally non-homogeneous with respect to time. The uniform continuous time average we used to obtain our proper orthogonal modes clearly has a big influence on the nature of the results, and we anticipate that averaging done over ensembles of impact Poincaré section data should result in larger numbers of modes, since one should expect more modes to be excited just after impact.

This work was supported by the Air Force Office of Scientific Research grant AFOSR-91-0430. We thank Matt Kennel for making the false nearest neighbours code of Kennel *et al.* (1992) available via anonymous ftp, and Charles Atz for making the code run on our recalcitrant workstation.

References

Breiman, L., Friedman, J. H., Olshen, R. A. & Stone, C. J. 1974 *Classification and regression trees*, p. 7. Belmont, California: Wadsworth International Group.

Cusumano, J. P. & Bai, B.-Y. 1993 Period-infinity periodic motions, chaos, and spatial coherence in a 10 degree of freedom impact oscillator. *Chaos solitons fractals* **3**, 515–536.

Everson, R. M. 1986 Chaotic dynamics of a bouncing ball. *Physica* D **19**, 355–383.

Foale, S. & Bishop, S. R. 1992 Dynamical complexities of forced impacting systems. *Phil. Trans. R. Soc. Lond.* A **338**, 547–556.

Franaszek, M. & Isomäki, H. M. 1991 Anomalous chaotic transients and repellers of the bouncing-ball dynamics. *Phys. Rev.* A **43**, 4231–4236.

Fraser, A. M. 1989 Information and entropy in strange attractors. *IEEE Trans. Information Theory* **35**, 245–262.

Fraser, A. M. & Swinney, H. L. 1986 Independent coordinates for strange attractors from mutual information. *Phys. Rev.* A **33**, 1134–1140.

Ghanem, R. G. & Spanos, P. D. 1991 *Stochastic finite elements: a spectral approach*. New York: Springer-Verlag.

Grassberger, P. & Procaccia, I. 1983 Characterization of strange attractors. *Phys. Rev. Lett.* **50**, 346–349.

Hendriks, F. 1983 Bounce and chaotic motion in print hammers. *IBM J. Res. Development* **27**, 273–280.

Holmes, P. J. 1992 The dynamics of repeated impacts with a sinusoidally vibrating table. *J. Sound Vib.* **84**, 173–189.

Kennel, M. B., Brown, R. & Abarbanel, H. D. I. 1992 Determining embedding dimension for phase-space reconstruction using a geometrical construction. *Phys. Rev.* A **45**, 3403–3411.

Kowalik, Z. J., Franaszek, M. & Pierański, P. 1988 Self-reanimating chaos in the bouncing-ball system. *Phys. Rev.* A **37**, 4016–4022.

Loève, M. 1963 *Probability theory*. Princeton, New Jersey: D. Van Nostrand.

Lumley, J. L. 1967 The structure of inhomogeneous turbulent flows. In *Atmospheric turbulence and radio wave propagation* (ed. A. M. Yaglom & V. I. Tatarski), pp. 166–178. Moscow: Nauka.

Mañé, R. 1981 On the dimension of the compact invariant sets of certain nonlinear maps. In *Dynamical systems and turbulence* (ed. D. A. Rand & L. S. Young). Springer Lecture Notes in Mathematics, **898**, 230–242. New York: Springer-Verlag.

Moon, F. C. 1992 *Chaotic and fractal dynamics: an introduction for applied scientists and engineers*. New York: John Wiley and Sons.

PHILOSOPHICAL TRANSACTIONS OF THE ROYAL SOCIETY A MATHEMATICAL, PHYSICAL & ENGINEERING SCIENCES

Moon, F. C. & Shaw, S. W. 1983 Chaotic vibration of a beam with nonlinear boundary conditions. *Int. J. Nonlinear Mech.* **18**, 465–477.

Nordmark, A. B. 1991 Non-periodic motion caused by grazing incidence in an impact oscillator. *J. Sound Vib.* **145**, 279–297.

Packard, N. H., Crutchfield, J. P., Farmer, J. D. & Shaw, R. S. 1980 Geometry from a time series. *Phys. Rev. Lett.* **45**, 712–716.

Shaw, S. W. 1985*a* The dynamics of a harmonically excited system having rigid amplitude constraints. Part I: subharmonic motions and local bifurcations. *ASME J. Appl. Mech.* **52**, 453–458.

Shaw, S. W. 1985*b* The dynamics of a harmonically excited system having rigid amplitude constraints. Part II: chaotic motions and global bifurcations. *ASME J. Appl. Mech.* **52**, 459–464.

Sirovich, L. 1987 Turbulence and dynamics of coherent structures. Part I: coherent structures. *Q. appl. Math.* **45**, 561–571.

Takens, F. 1981 Detecting strange attractors in turbulence. In *Dynamical systems and turbulence* (ed. D. A. Rand & L. S. Young). Springer Lecture Notes in Mathematics, **898**, 266–281. New York: Springer-Verlag.

Tufillaro, N. B. & Albano, A. M. 1986 Chaotic dynamics of a bouncing ball. *Am. J. Phys.* **54**, 939–944.

Whiston, G. S. 1987 Global dynamics of a vibro-impacting linear oscillator. *J. Sound Vib.* **118**, 395–429.

Whiston, G. S. 1992 Singularities in vibro-impact dynamics. *J. Sound Vib.* **152**, 427–460.

PHILOSOPHICAL TRANSACTIONS OF THE ROYAL SOCIETY A MATHEMATICAL, PHYSICAL & ENGINEERING SCIENCES